

Supporting Information

Piezochromism and Anomalous Near-Infrared Luminescence Evolution of BaCuSi₄O₁₀ and BaCuSi₂O₆ via Pressure-Induced Phase Transition

Ke Liu,^a Chen Li,^a Dequan Jiang,^b Yingying Ma,^a Ting Wen,^{*a} Binbin Yue^a and Yonggang Wang^b

^aCenter for High Pressure Science and Technology Advanced Research (HPSTAR), Beijing 100193, China.

^bSchool of Materials Science and Engineering, Peking University, Beijing 100871, China.

* E-mail: ting.wen@hpstar.ac.cn

Figure S1. Rietveld refinement results of BaCuSi₄O₁₀ powder XRD patterns at ambient condition.

Figure S2. Rietveld refinement results of BaCuSi₂O₆ powder XRD patterns at ambient condition.

Figure S3. NIR emission spectra of BaCuSi₄O₁₀ and BaCuSi₂O₆ at ambient condition.

Figure S4. The decay time of BaCuSi₄O₁₀ and BaCuSi₂O₆ at ambient condition.

Figure S5. NIR emission spectra of BaCuSi₄O₁₀ at 0.3 GPa and after pressure release.

Figure S6. NIR emission spectra of BaCuSi₂O₆ at 0.4 GPa and after pressure release.

Figure S7. LeBail fitting results of BaCuSi₄O₁₀ at (a) 0.2 GPa, (b) 3.1 GPa, and (c) 17.3 GPa.

Figure S8. XRD patterns of BaCuSi₄O₁₀ at 0.2 GPa and after pressure release.

Figure S9. The Raman spectra of BaCuSi₄O₁₀ at 0.4 GPa and after pressure release.

Figure S10. LeBail fitting results of BaCuSi₂O₆ at (a) 0.2 GPa, (b) 14.7 GPa.

Figure S11. (a) *In situ* HP cell parameters of BaCuSi₂O₆ under selected pressure, and (b) the cell volume as a function of applied pressure.

Figure S12. *in situ* HP Raman spectra of BaCuSi₂O₆.

Figure S13. XRD patterns of BaCuSi₂O₆ at 0.2 GPa and after pressure release.

Figure S14. The Raman spectra of BaCuSi₂O₆ at 0.3 GPa and after pressure release.

Figure S15. Optical photos of BaCuSi₂O₆ during compression.

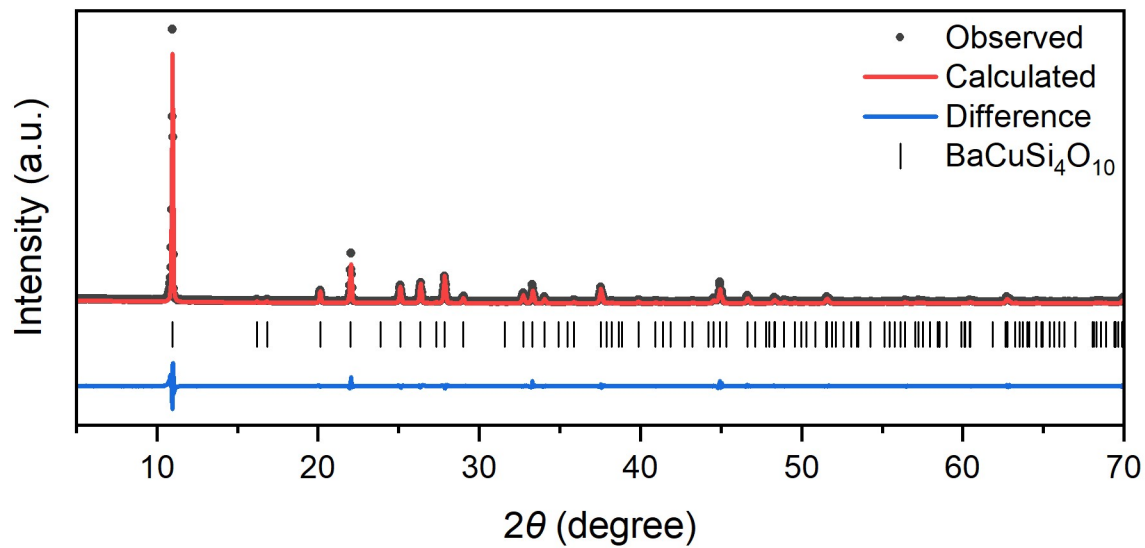


Figure S1. Rietveld refinement results of BaCuSi₄O₁₀ powder XRD patterns at ambient condition.

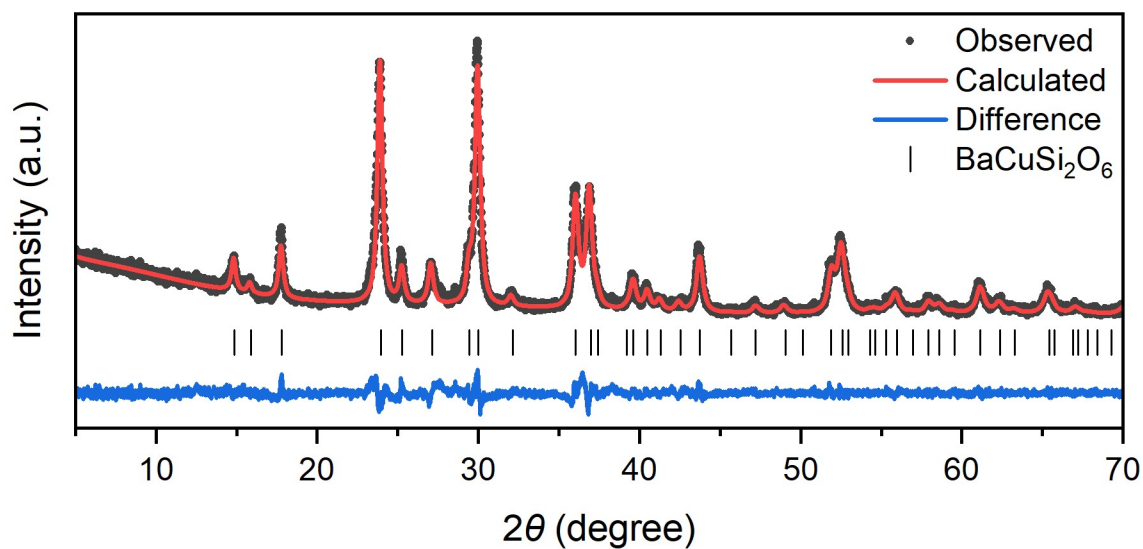


Figure S2. Rietveld refinement results of BaCuSi₂O₆ powder XRD patterns at ambient condition.

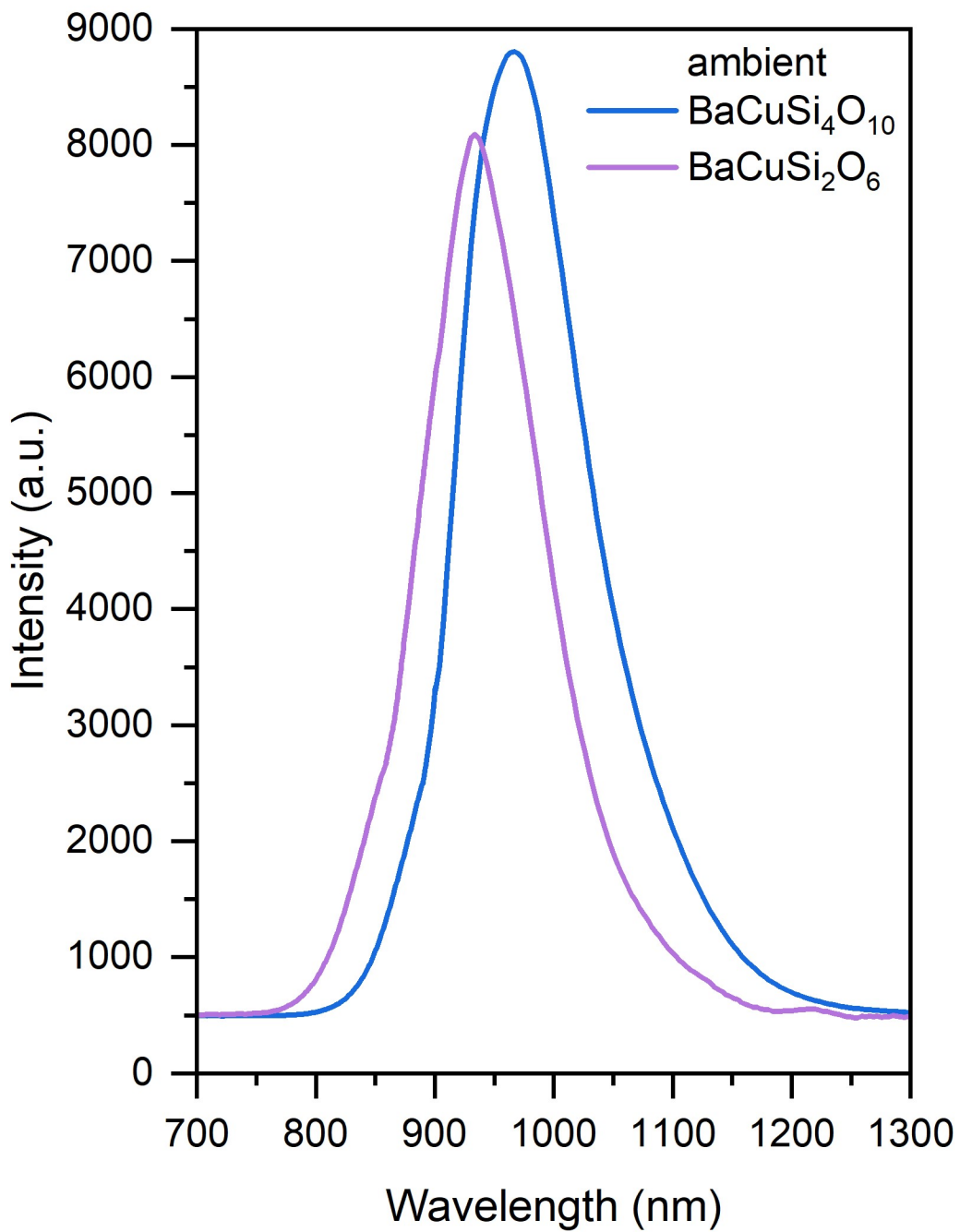


Figure S3. NIR emission spectra of BaCuSi₄O₁₀ and BaCuSi₂O₆ at ambient condition.

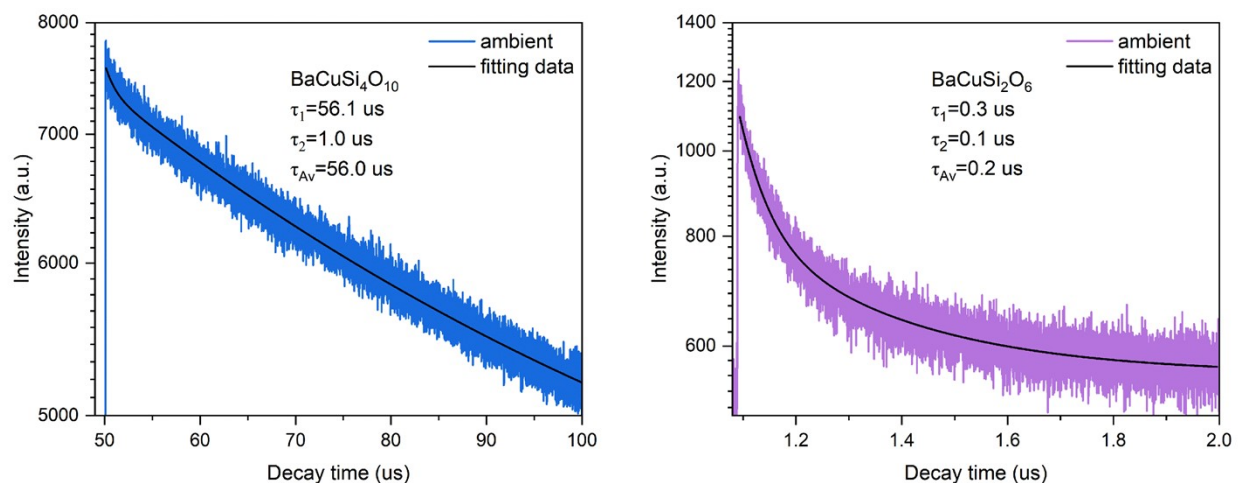


Figure S4. The decay time of BaCuSi₄O₁₀ and BaCuSi₂O₆ at ambient condition.

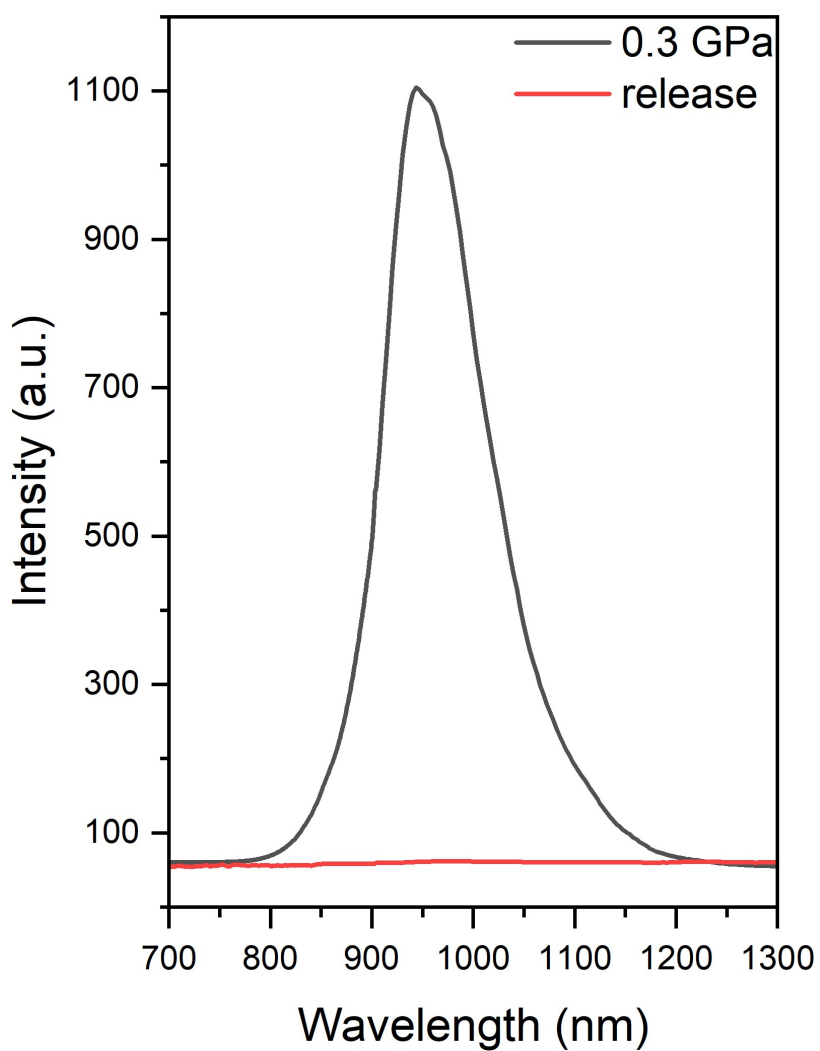


Figure S5. NIR emission spectra of BaCuSi₄O₁₀ at 0.3 GPa and after pressure release.

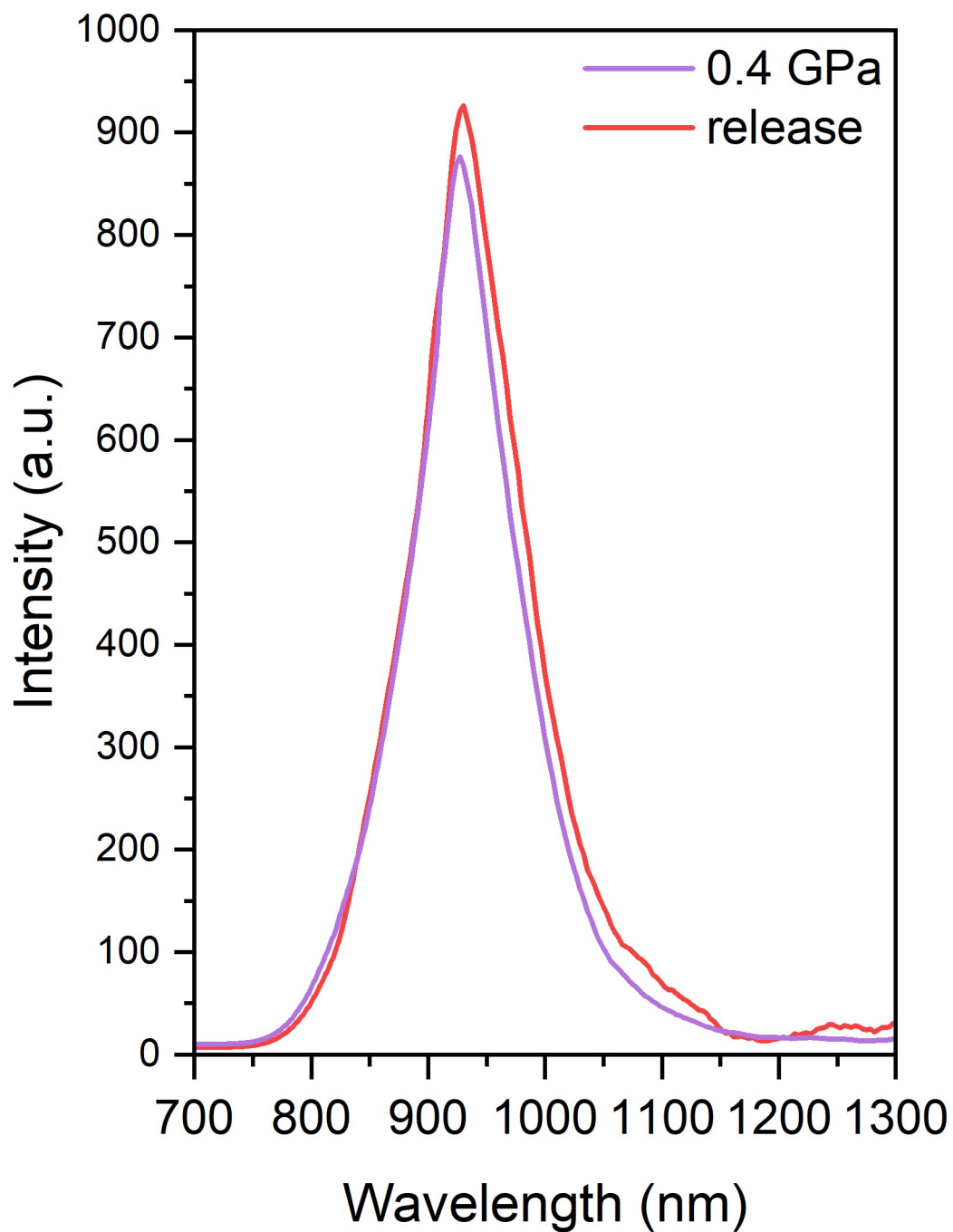


Figure S6. NIR emission spectra of BaCuSi₂O₆ at 0.4 GPa and after pressure release.

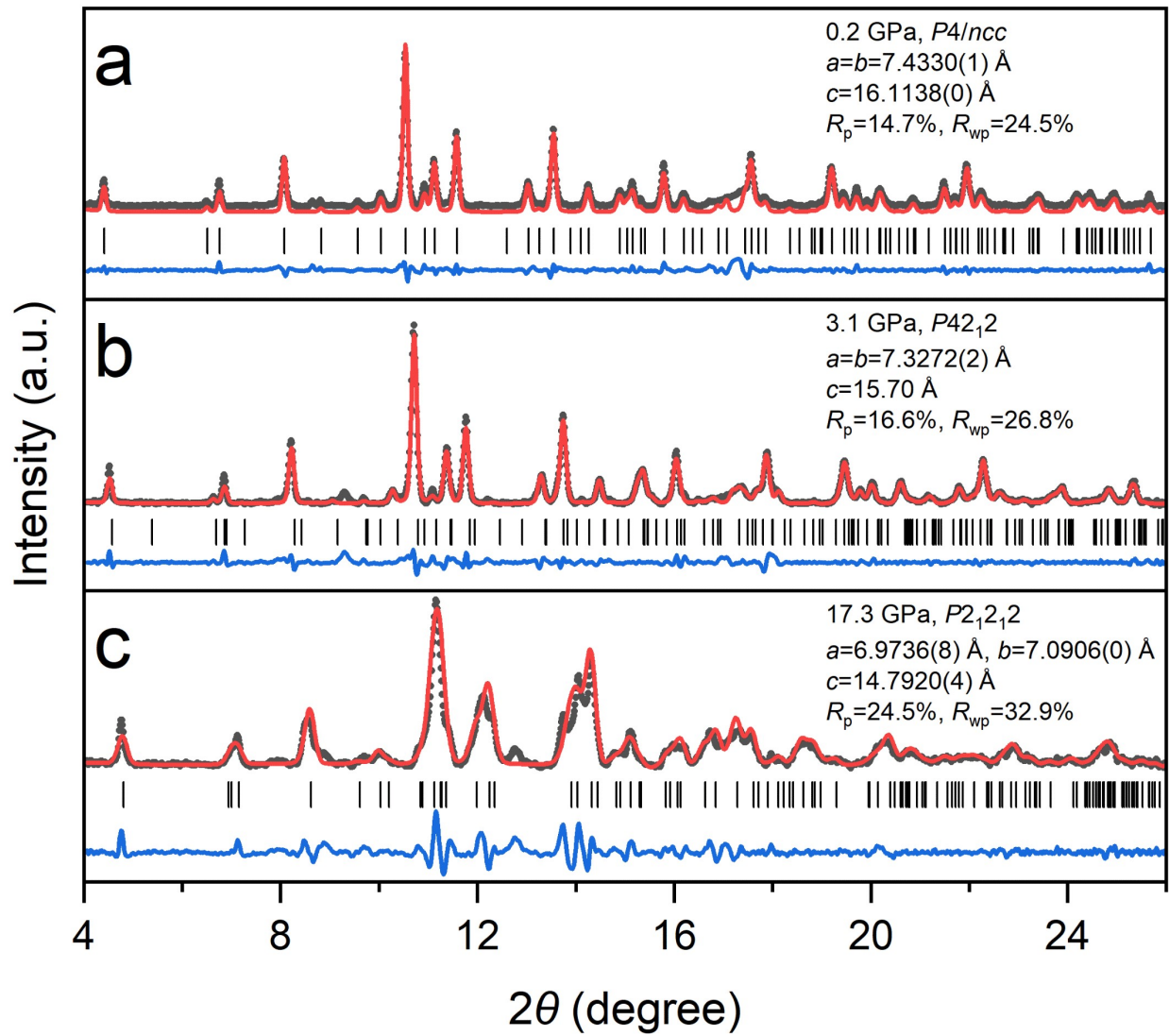


Figure S7. LeBail fitting results of BaCuSi₄O₁₀ at (a) 0.2 GPa, (b) 3.1 GPa, and (c) 17.3 GPa.

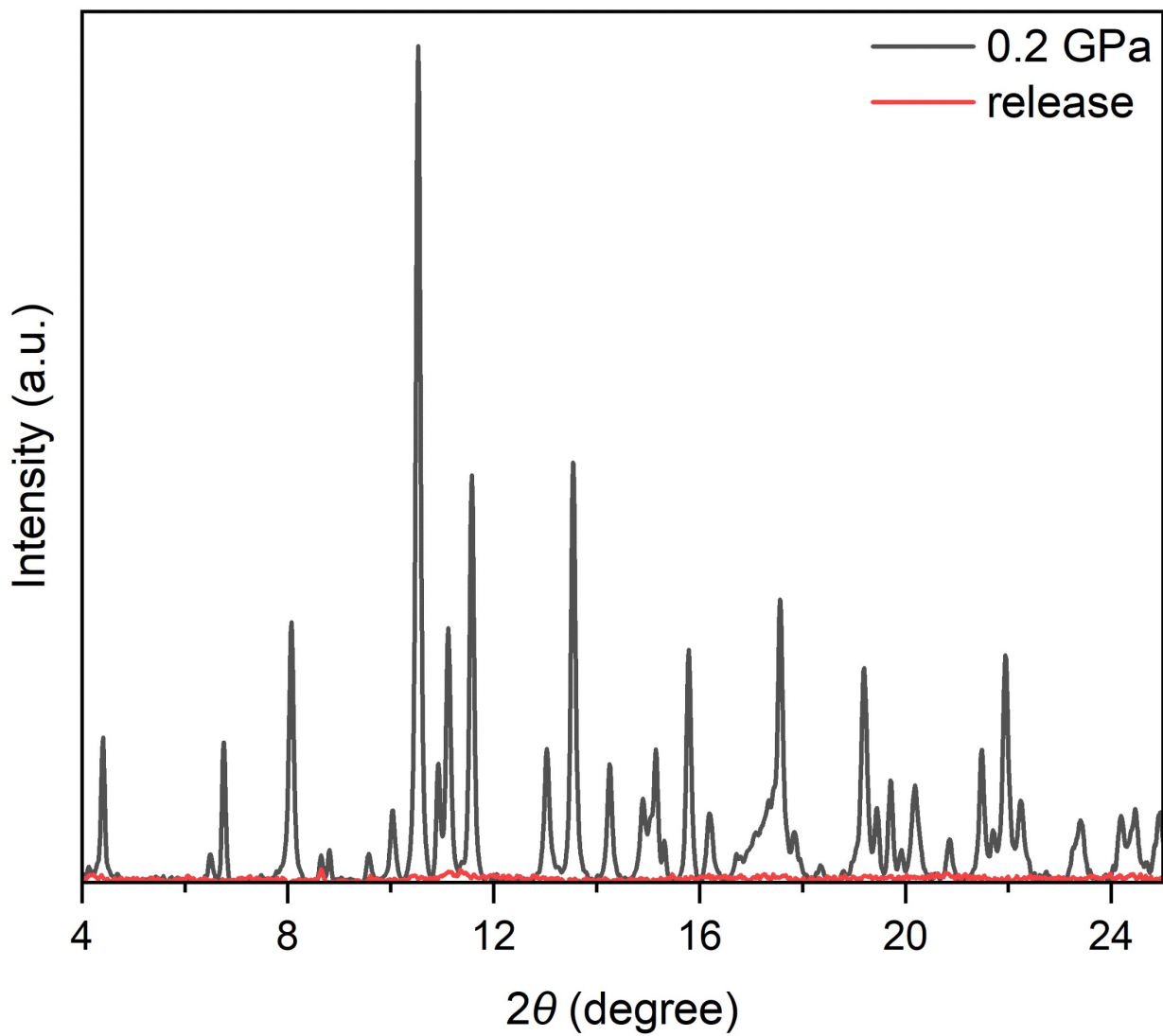


Figure S8. XRD patterns of BaCuSi₄O₁₀ at 0.2 GPa and after pressure release.

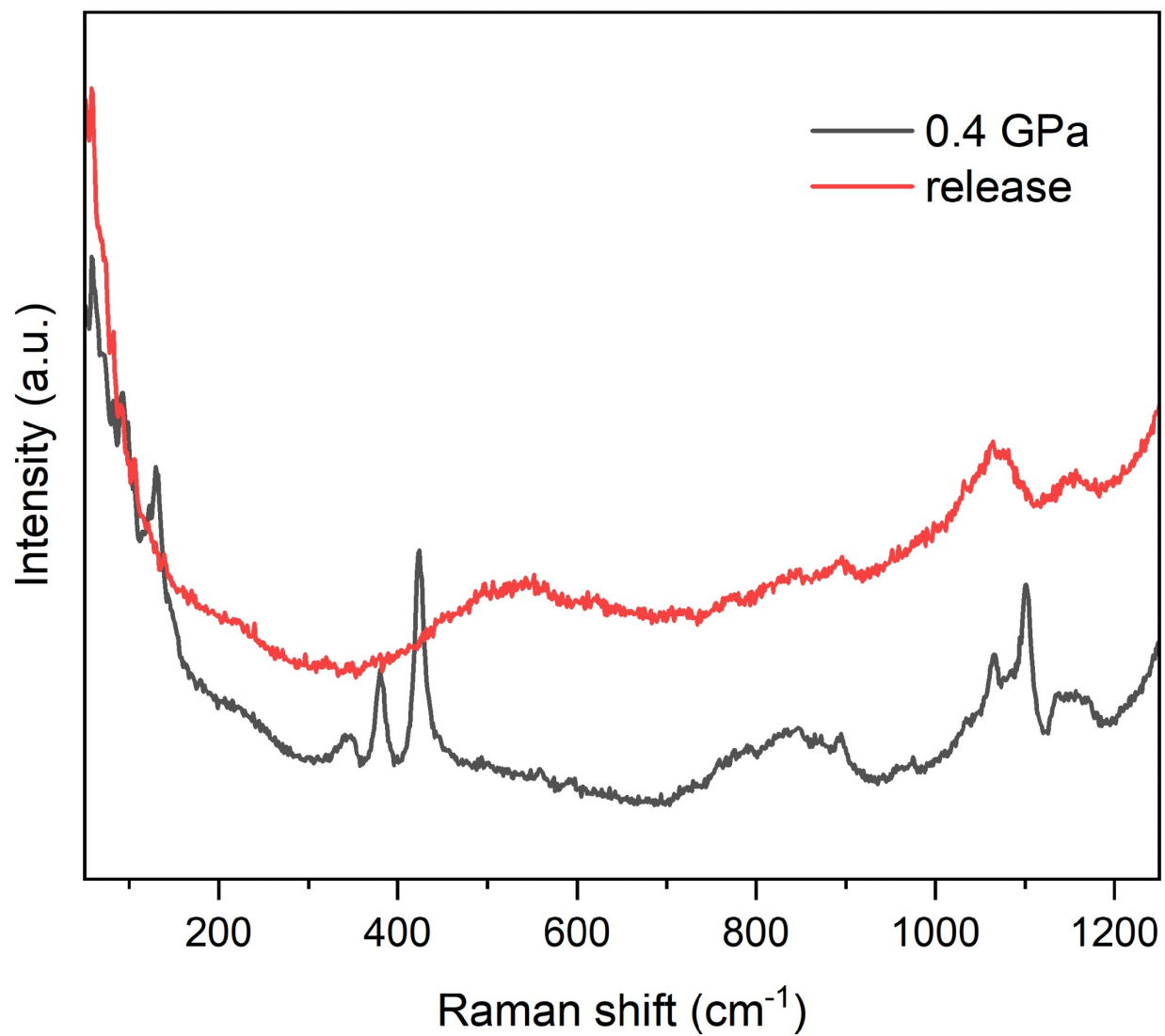


Figure S9. The Raman spectra of BaCuSi₄O₁₀ at 0.4 GPa and after pressure release.

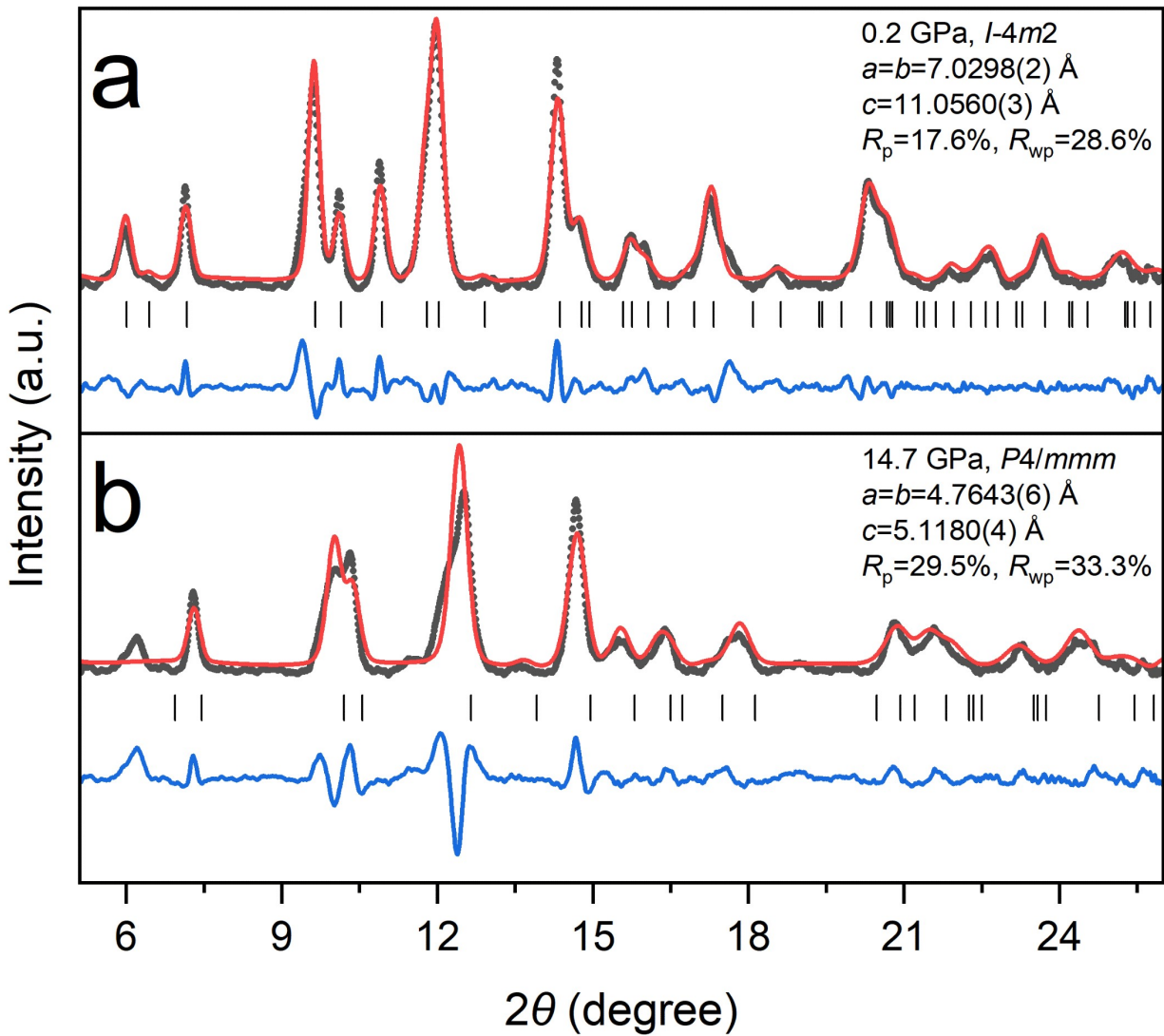


Figure S10. LeBail fitting results of BaCuSi₂O₆ at (a) 0.2 GPa, (b) 14.7 GPa.

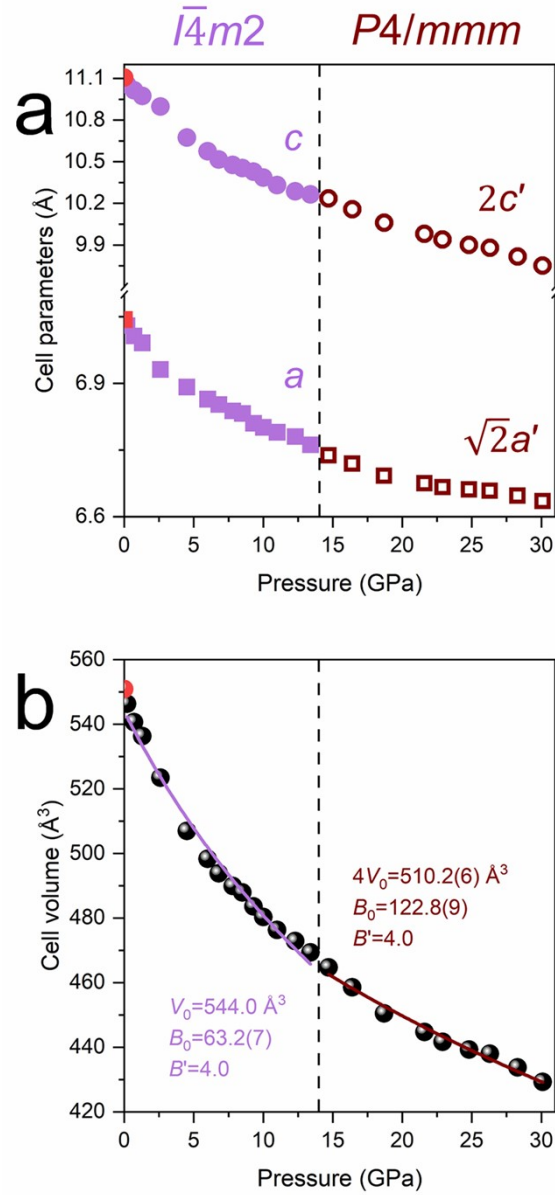


Figure S11. (a) *In situ* HP cell parameters of BaCuSi₂O₆ under selected pressure, and (b) the cell volume as a function of applied pressure.

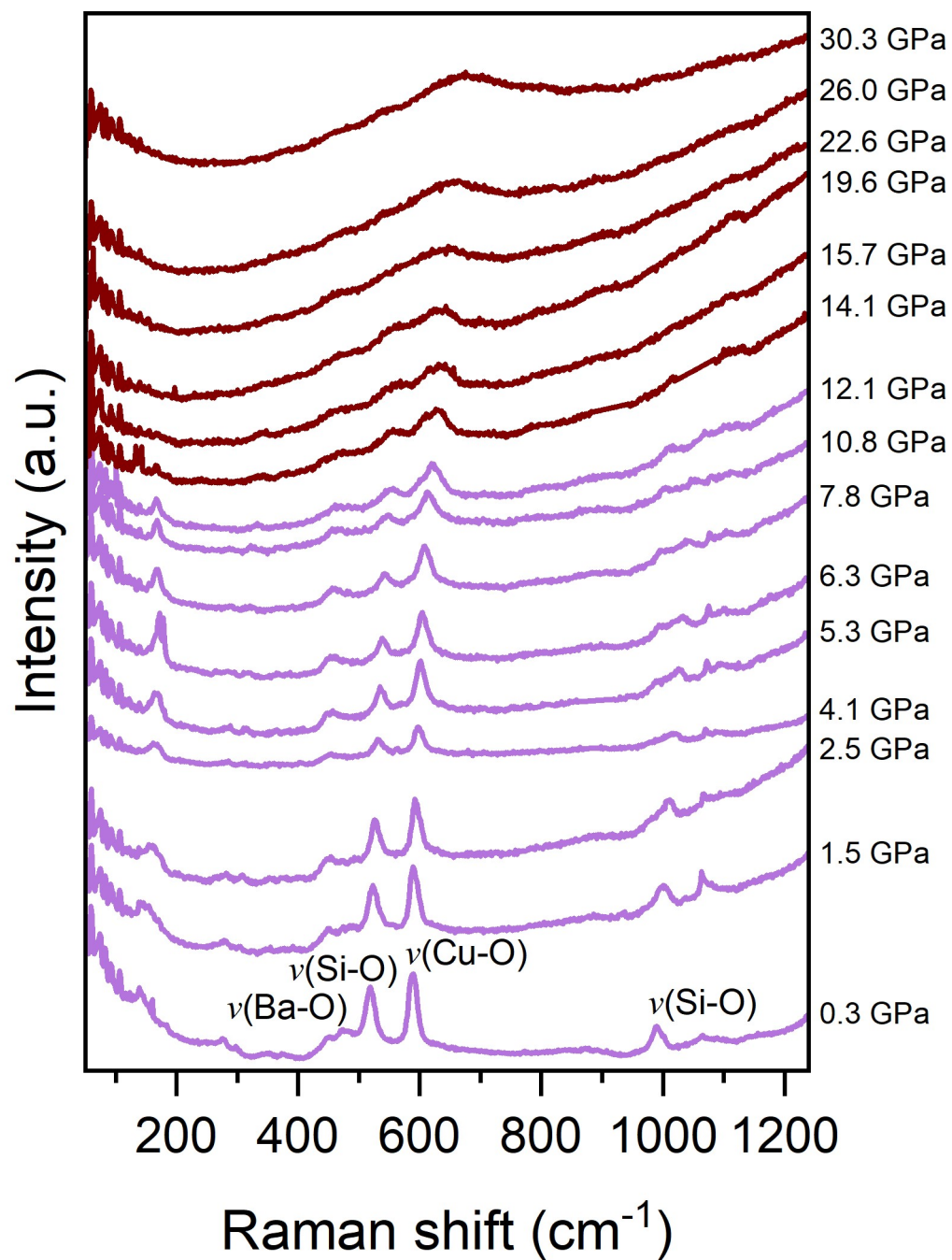


Figure S12. *in situ* HP Raman spectra of BaCuSi₂O₆.

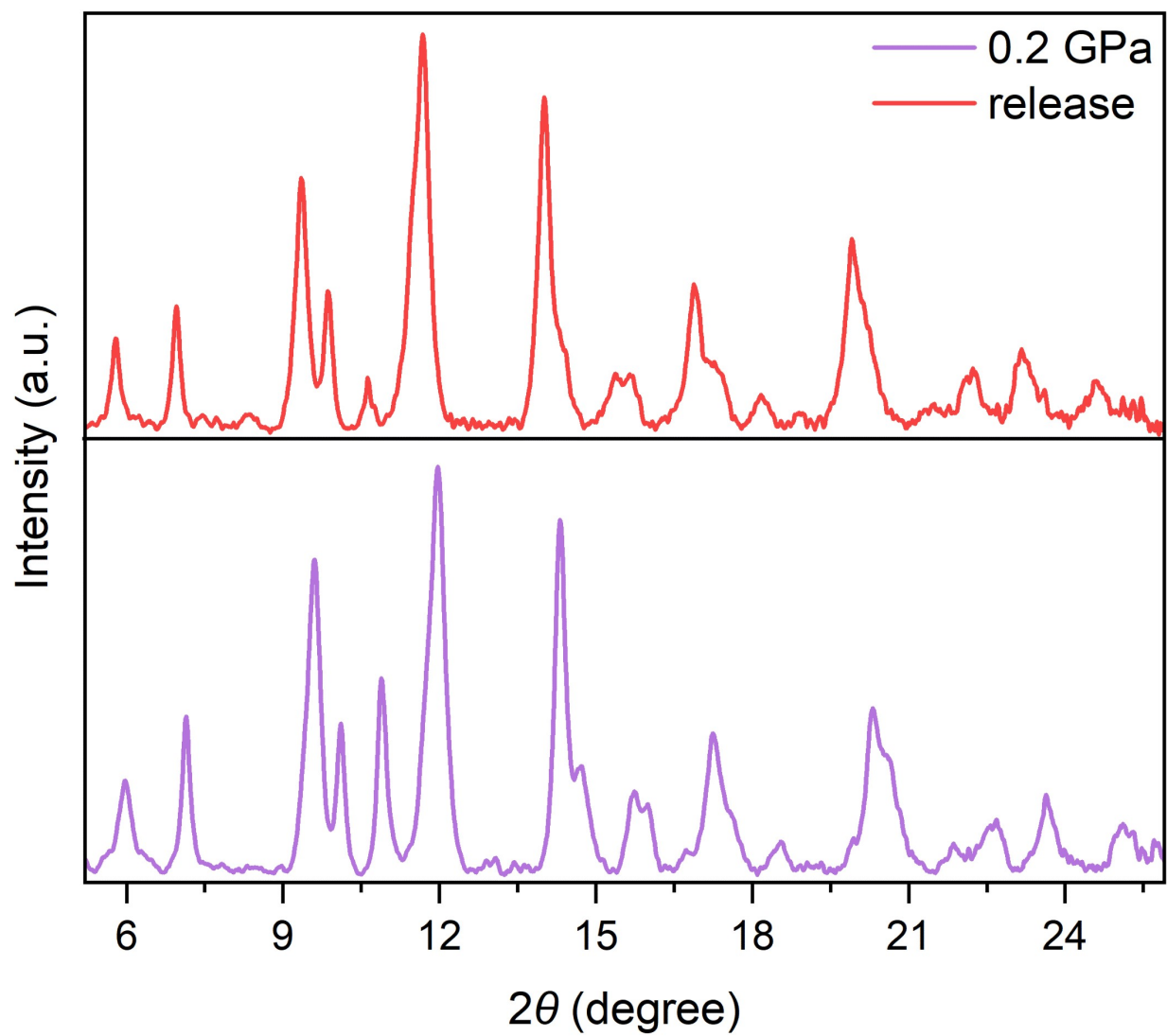


Figure S13. XRD patterns of BaCuSi₂O₆ at 0.2 GPa and after pressure release.

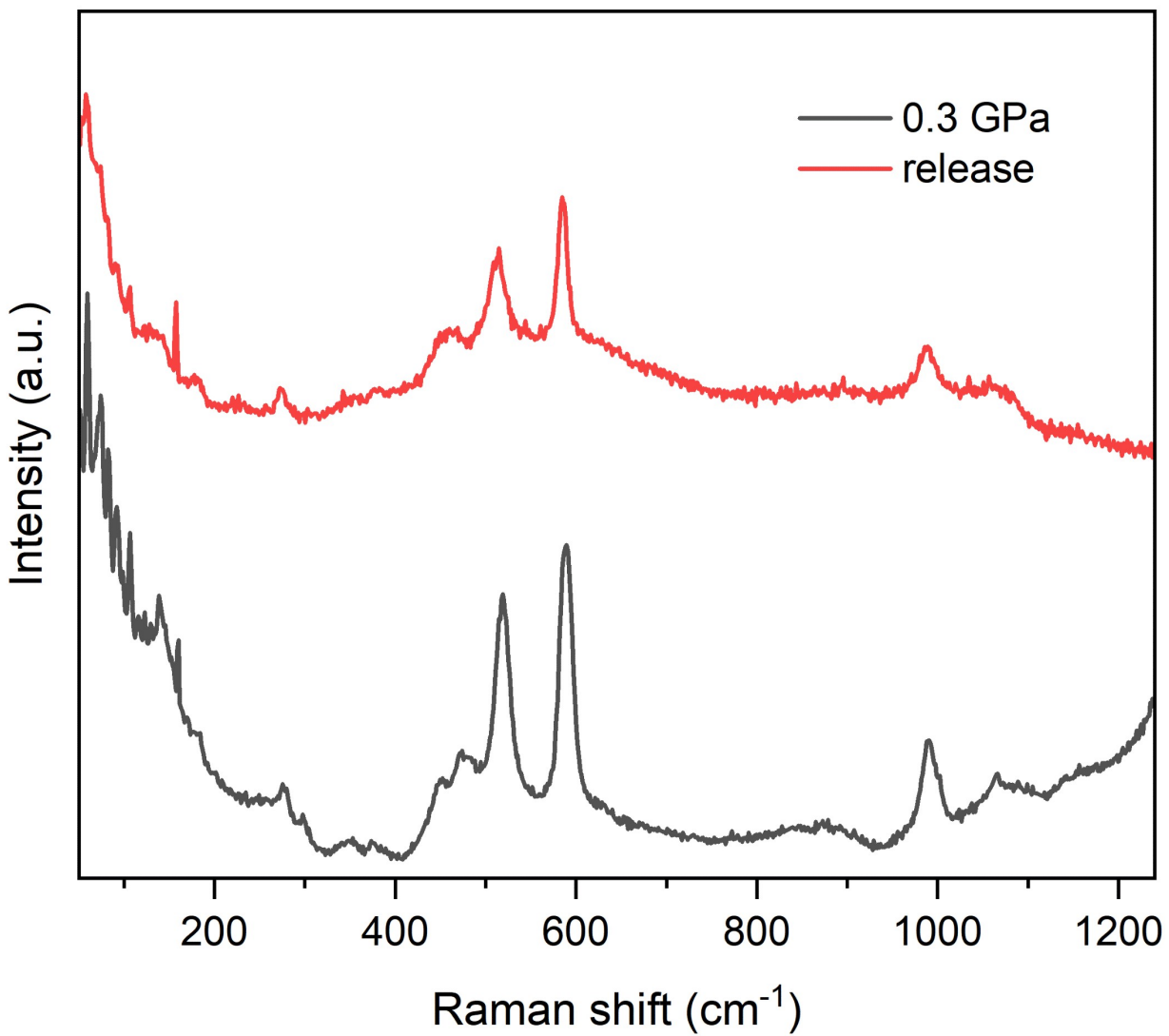


Figure S14. The Raman spectra of BaCuSi₂O₆ at 0.3 GPa and after pressure release.

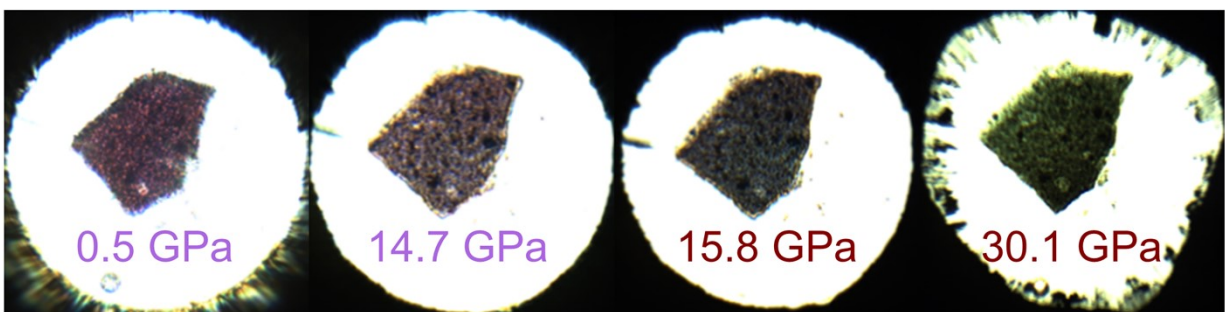


Figure S15. Optical photos of BaCuSi₂O₆ during compression.